An approach to numerical simulation of the gas distribution in the atmosphere of Enceladus

V. Tenishev,[1] M. R. Combi,[1] B. D. Teolis,[2] and J. H. Waite[2]

Received 21 December 2009; revised 9 March 2010; accepted 19 April 2010; published 2 September 2010.

[1] In addition to being the major source of neutral gas and dust particles for the Saturnian E-ring and, ultimately, heavy ions for the Saturnian inner magnetosphere, Enceladus exhibits geological activity that has made it an object of recent intensive study. The interest has significantly increased after Cassini flybys in 2005 provided a detailed map of its surface, showing that most of its activity occurs in a region around the south pole of the satellite. Dust jets that were discovered during the flybys can be related to a set of localized gas sources that dominate the supply of material into the rarefied atmosphere of Enceladus. A comprehensive data analysis involves developing physical models that include all major processes occurring in the atmosphere. Such models can be used not only for calibration and understanding of data already available, but also could have a practical application for planning upcoming flybys. This work presents the results of the development and application of a kinetic model of the Enceladus' atmosphere consisting of a gas described in terms of its distribution function. The paper describes the basic principles of the model and gives a comparison with the observational data obtained with Cassini instruments.

Citation: Tenishev, V., M. R. Combi, B. D. Teolis, and J. H. Waite (2010), An approach to numerical simulation of the gas distribution in the atmosphere of Enceladus, *J. Geophys. Res.*, *115*, A09302, doi:10.1029/2009JA015223.

1. Introduction

[2] Due to its small size and proximity to Saturn that complicates ground based observations, our knowledge of Enceladus, an icy Saturnian satellite discovered in 1789, was very limited for a long time.

[3] The Voyager 1 spacecraft was the first to study Enceladus. During its journey through the Saturnian system, the first images of the Enceladus' surface [*Terrile and Cook*, 1981; *Buratti et al.*, 1990] were obtained. The absence of visual topographic features on its highly reflective surface and the fact that it consists mostly of water ice was an unexpected result. These features suggest that significant tidal heating [*Smith et al.*, 1981; *Meyer and Wisdom*, 2007] and possible volcanic activity [*Squyres et al.*, 1983; *Owen et al.*, 1986; *Dermott and Thomas*, 1994] has led to recent resurfacing.

[4] It was known for a long time that Enceladus orbits [*Harper and Taylor*, 1993] within the E-ring, the outermost Saturnian ring located between $3R_\mathfrak{h}$ and $8R_\mathfrak{h}$ and composed [*Showalter et al.*, 1991; *Hillier et al.*, 2007] mostly of small icy particles with an average size of $\sim 1\mu$m. During the Voyager 1 mission it was found that the position of Enceladus is located [*Baum et al.*, 1981] in the region of maximum brightness of the ring.

[5] Assuming Enceladus to be the major source of material for the E-ring, *Terrile and Cook* [1981] estimated that the dust production rate of the order of ~ 0.1 g s^{-1} is required to maintain the present density of the ring. More recently, Enceladus was linked to the existence of a substantial OH cloud that was found [*Shemansky et al.*, 1993; *Hall et al.*, 1996; *Jurac et al.*, 2002] with HST observations at a distance of $\sim 4.5R_\mathfrak{h}$ from Saturn.

[6] Voyager 2 images of Enceladus' surface have indicated [*Squyres et al.*, 1983] the existence of regions with highly varying geological ages as evidenced by the distribution of craters on its surface. Using images obtained with the Imaging Science Subsystem (ISS) onboard of Cassini, *Porco et al.* [2006] have determined the radius of Enceladus to be 252 km and the mean density of $\rho = 1.6$ g cm^{-3}.

[7] During the 2005 flyby, the Cassini spacecraft approached [*Porco et al.*, 2006; *Brown et al.*, 2006; *Spencer et al.*, 2006; *Dougherty et al.*, 2006; *Spahn et al.*, 2006] Enceladus and passed within 175 km of its surface. This allowed a direct measurement [*Jones et al.*, 2006; *Waite et al.*, 2006] of its dusty gas environment with instruments onboard of the spacecraft. The atmosphere of Enceladus was found [*Waite et al.*, 2006] to consist mostly of water with some fraction of CO_2, CO and/or N_2, and CH_4. Gas production is concentrated in the south pole region, in the vicinity of long cracks, the so called "Tiger stripes", discovered [*Porco et al.*, 2006] from Cassini images. The cracks are characterized [*Spencer et al.*, 2006] by an anomalously high surface temperature. Locations of regions with a higher surface temperature can be related to the origin [*Hansen et al.*, 2008] of the observed gas and dust jets.

[1]Department of Atmospheric, Oceanic and Space Sciences, University of Michigan, Ann Arbor, Michigan, USA.
[2]South-West Research Institute, San Antonio, Texas, USA.

Copyright 2010 by the American Geophysical Union.
0148-0227/10/2009JA015223

Table 1. Position and Direction of Enceladus' Dust Jets[a]

Source	Tiger Stripe	Position on the Surface		Direction of the Dust Jets	
		Lat.[b]	W. Lon.[b]	Zenith Angle[c]	Azimuth Angle[d]
I	Baghdad	81.5	31.2	9.7	228.7
II	Damascus	79.2	313.2	6.8	93.8
III	Damascus	81.2	294.2	30.2	83.2
IV	Alexandria	73.2	148.4	3.7	110.0
V	Cairo	78.7	72.6	6	229.8
VI	Baghdad	87.1	237.0	10.2	187.6
VII	Baghdad	74.7	28.9	20.8	352.5
VIII	Cairo	82.1	115.5	6.8	127.7

[a]The table is taken from *Spitale and Porco* [2007].
[b]Latitudes (Lat.) are planetographic and longitudes (W. Lon.) increase toward the west.
[c]Zenith angle is measured in degrees between the vertical direction and the direction of the plume.
[d]Azimuth angle is measured in degrees clockwise from local north (that is, eastward to an observer standing on the surface facing north).

[8] In this paper we have developed models for numerical reconstruction of the atmosphere of Enceladus to explain the data collected with the Ultraviolet Imaging Spectrograph (UVIS) [*Hansen et al.*, 2006] and the Ion and Neutral Mass Spectrometer (INMS) [*Waite et al.*, 2006] instruments. First, the multi-plume semi-analytical model was used to determine parameters of Enceladus' gas production by fitting INMS and UVIS data. Then, a test particle Monte-Carlo model is used to check the importance of Enceladus' gravity in determining the density distribution within its atmosphere. The principal difference of the models presented here from those developed by other authors [*Jurac et al.*, 2002; *Waite et al.*, 2006; *Burger et al.*, 2007; *Tian et al.*, 2007; *Matson et al.*, 2007] is a fully three-dimensional treatment of the atmosphere that allows us to include a set of gas sources located at the points of origin of the observed jets [*Porco et al.*, 2006; *Spitale and Porco*, 2007].

[9] The INMS data presented in this paper contains an overall factor of three correction upward that has been found since the initial report by *Waite et al.* [2006].

2. Model Study of Neutral Components in Enceladus' Atmosphere

[10] Due to the low density everywhere except the innermost vicinity of the vents, the gas can be considered to be collisionless. As a result, methods of computational fluid dynamics are not applicable here and the flow must be studied by solving [*Aristov*, 2001] the Boltzmann equation. All the models developed to date actually solve some form of the Boltzmann equation with different variations of the Monte Carlo approach.

[11] A model reproducing the INMS data was presented by *Waite et al.* [2006], where the total gas production was split between a localized source around the south pole region and a uniform source over the whole surface of Enceladus. Assuming the value of the bulk speed in the flow to be about 400 m s^{-1}, fitting of the observational data yielded a uniform source rate on the order of $S_1 \approx 1.2 \times 10^{26}$ s^{-1}. The rate of gas production due to a source concentrated around the south pole of Enceladus was estimated at a temperature of $T = 190$ K to be about $S_2 \approx 1.7 \times 10^{26}$ s^{-1}. Variation of the temperature in a range from 140 K to 270 K introduces a variation of 20% to the source strength. The total gas production rate was found to be in the range from $S \approx 1.7 \times 10^{26}$ to 5.0×10^{26} s^{-1}.

[12] A test particle Monte-Carlo model of a neutral gas distribution in Enceladus' atmosphere was presented by *Burger et al.* [2007], where the gas production is considered to be split among a spherically uniform source and a source localized around the south pole. The first one accounts for water injected uniformly from the surface of Enceladus and a background torus, in which the density was assumed to be $\sim 1.6 \times 10^4$ cm^{-3}. Simultaneously fitting the INMS and UVIS data, water production rates of $S_1 \approx 8 \times 10^{25}$ s^{-1} and $S_2 \approx 10^{28}$ s^{-1} were obtained for the uniform and localized sources, respectively.

[13] Studying the distribution of density within the OH torus obtained with HST observations, *Jurac et al.* [2002] have found that a water source rate of 3.75×10^{27} s^{-1} is required to maintained the observed torus density. Using a Monte Carlo model of the neutral torus, *Richardson and Jurac* [2004] suggests the value of 10^{28} s^{-1} for the water source. Direct ejection of water should account for [*Tokar et al.*, 2006] about 80% of the total OH source.

[14] An analysis of the UVIS data set by *Hansen et al.* [2006] indicates that the total water escape rate is at least 5×10^{27} s^{-1}. Using a test particle Monte-Carlo approach to simulate the UVIS data, *Tian et al.* [2007] later determined the total escape rate of water to be $\sim(4\text{–}6) \times 10^{27}$ s^{-1}. Mechanisms of possible origin of the minor species in the plume are considered by *Matson et al.* [2007].

[15] In addition to studying the neutral distribution directly ejected from Enceladus, a Monte Carlo approach has also been used to simulate formation of a torus that is composed of products of water photo-dissociation and is located in the vicinity of the Enceladus' orbit. The results of those efforts are described by *Johnson et al.* [2006] and *Jurac et al.* [2002].

2.1. Semi-Analytical Multi-Plume Model

[16] Currently available data of the gas production is not sufficient to formulate unique boundary conditions that would allow one to reproduce uniquely the volume distribution of the gas' microscopic parameters in the atmosphere of Enceladus. For this reason, an analysis of the available data requires developing a fitting procedure that is based on some assumptions on a structure of boundary conditions and allows reconstruction of the data observed with the UVIS and INMS instruments.

[17] Studying the Cassini Composite Infrared Spectrometer (CIRS) data, *Spitale and Porco* [2007] have determined positions of jet source locations that are listed in Table 1. In our model, gas vents are associated with those locations. Production of the gas injected into the atmosphere of Enceladus is due to the vents together with a spherically uniform source, for which parameters are obtained by fitting to the available data.

[18] A numerical simulation of the density distribution has shown that the gas is in a collision dominated regime only in the innermost region around the vents, which allows them to be considered independently. Due to a high collision rate, the gas becomes thermalized in the vicinity of a vent. Since the primary interest is the density distribution at distances

Table 2. Total Plume and Spherical Source Rates

Case	Spherical Source[a]	Plume Source[b]
Case 1[c]	3.6×10^{25}	4.2×10^{28}
Case 2[d]	4.7×10^{25}	2.6×10^{28}

[a]The gas production is measured in s^{-1}.
[b]The Plume Source is a sum of production rates of all plumes and is measured in s^{-1}.
[c]Case 1 is a fit to the original INMS E3, E5 and UVIS E2 data.
[d]Case 2 is the fit to the sticking model processed INMS E3, E5 data and the original UVIS E2 data.

that are much larger than the characteristic size of the collision-dominated region around a vent, each of them is considered here as a point source with an injected gas distributed according to a convected Maxwell-Boltzmann distribution in the form $f(\mathbf{v}) = A_p \exp(-\beta^2(\mathbf{v} - \mathbf{v}_p)^2)$, where $\beta = \sqrt{(m/2kT_p)}$, A_p is a normalization constant, T_p and $\mathbf{v}_p$ are the temperature and the bulk velocity of the gas flow in the vicinity of the vent, respectively. This represents the state of the gas in the innermost vicinity of each vent.

[19] Expansion of a gas from a point source can be described analytically by solving the Liouville equation. Since the mean molecular speed in the flow exceeds the escape speed of Enceladus (235 m s^{-1}), in a first approximation the gravity force can be excluded from consideration. That allows each jet to be axially symmetrical. This greatly simplifies the problem and minimizes the number of free parameters.

[20] It is more convenient to consider each jet in a spherical coordinate frame originating at the jet location and with the $\hat{z}$-axis coinciding with a direction of the jet. Taking azimuthal and zenith angles to be ϕ and θ, respectively, the velocity distribution in the vicinity of a vent can be expressed as $f_p(v, \phi, \theta) = A_p v^2 \exp(-\beta^2((v \sin\theta - v_p)^2 + v^2 \cos^2\theta))\cos\theta$, where A_p and v_p are the normalization constant and the bulk speed associated with the jet, respectively. The normalization constant is related to the value of the production rate of the jet $F_p = \int v f_p(v, \phi, \theta) d\phi d\theta dv$. The density due to the jet outside of the vent can be evaluated as $n_p(r, \phi, \theta) = r^{-2} \int f_p(v, \phi, \theta)/\cos\theta dv$, where r is the distance from the origin of the vent.

[21] The requirement for non-intersection of the surface by an injected particle, $(\mathbf{v}(\phi, \theta), \mathbf{r}_p) \geq 0$, limits the variation of azimuthal and zenith angles. Here, $\mathbf{v}(\phi, \theta)$ is the velocity of an injected particle, $\mathbf{r}_p$ is the location of the vent in a coordinate frame related to the center of Enceladus and $(\cdot, \cdot)$ is a scalar product of two vectors.

[22] In the model presented here, eight independent vents listed in Table 1 and a uniform source are used to describe a gas production of Enceladus. Each vent is characterized by temperature, production rate, direction and bulk velocity of a gas flow in its innermost vicinity. The density distribution due to a spherical source is taken in the form of $n(r) = c_0 + c_1/r^2$, where c_0 and c_1 are empirical constants that have to be found by a fitting procedure, and r is the distance from the center of Enceladus.

2.2. Test Particle Monte Carlo Model

[23] The most important force that governs motion of gas molecules outside of a vent is the gravity of Enceladus. The analytical approach for the density distribution cannot account for the gravity because it will destroy the axial symmetry of a jet implicitly embedded into the model.

[24] To check the effect of gravity on the distribution of macroscopic parameters within the Enceladus' atmosphere, we have developed a test particle Monte-Carlo model that can simulate the density distribution using parameters obtained by the semi-analytical multi-plume model.

3. Results and Discussion

[25] We use the semi-analytical model to determine the parameters of the jets and the spherical source by fitting them to known profiles of number and column densities. In the following, we will use two sets of data to fit the model that will be referred to as case 1 and case 2. In case 1, the model parameters are determined by fitting to the original INMS E3 and E5 and UVIS E2 data. In case 2, the INMS E3 and E5 data were first preprocessed with a sticking model [*Teolis et al.*, 2010] that accounts for the temporary sticking of water molecules inside the INMS antechamber in front of the closed source.

3.1. Semi-Analytical Multi-Plume Model

[26] The model was used to fit parameters of eight independent plumes and a uniform spherical source for both cases. Positions of the plumes [*Spitale and Porco*, 2007] are listed in Table 1 and were fixed. Parameters of the Maxwell-Boltzmann distribution and direction of each plume were determined by a fitting procedure.

[27] Source rates of the uniform spherical source for both cases are listed in Table 2 and vary in the range $S_1 \approx (3.6\text{–}4.7) \times 10^{25}$ s^{-1}, which is compatible with those obtained by *Waite et al.* [2006] and *Burger et al.* [2007].

[28] The total production rate of the plumes for the cases considered falls in the range $S_2 \approx (2.6\text{–}4.2) \times 10^{28}$ s^{-1}. Dominated by the plumes, the resulting value of the total gas production rate into the Enceladus atmosphere, $S = S_1 + S_2$, exceeds that of *Waite et al.* [2006] but is in a good agreement with a source rate obtained by *Burger et al.* [2007], *Jurac et al.* [2002], *Tokar et al.* [2006], *Hansen et al.* [2006] and *Tian et al.* [2007]. Obtained with the fitting procedure, directions of the plumes are very close to those determined by *Spitale and Porco* [2007].

Table 3. Model Parameters of the Most Important Plumes for Case 1[a]

Plume	Source Rate[b]	Bulk Velocity[c]	Opening Angle[d]	Zenith Angle[e]	Azimuth Angle[f]
I	1.1×10^{28}	6.1×10^2	37	4.7	209
II	4.9×10^{27}	7.0×10^2	26	5.0	73.8
III	5.6×10^{27}	7.0×10^2	27	25	63.2
VII	1.9×10^{28}	7.0×10^2	36	16	12.5

[a]The model is fitted to the original INMS E3, E5 and UVIS E2 data.
[b]A plume sources rate is measured in s^{-1}.
[c]Bulk velocity of a gas in a plume in a vicinity of the surface is measured in ms^{-1}.
[d]Opening angle is defined by equation (1) and is measured in degrees.
[e]Zenith angle is measured in degrees between the vertical direction and the direction of the plume.
[f]Azimuth angle is measured in degrees clockwise from local north (that is, eastward to an observer standing on the surface facing north).

Table 4. Model Parameters of the Most Important Plumes for Case 2[a]

Plume	Source Rate[b]	Bulk Velocity[c]	Opening Angle[d]	Zenith Angle[e]	Azimuth Angle[f]
I	2.1×10^{26}	6.4×10^{2}	30	9.0	223
II	7.8×10^{27}	7.0×10^{2}	29	8.7	73.8
III	5.8×10^{27}	7.0×10^{2}	26	25	63.2
VII	1.3×10^{28}	5.2×10^{2}	42	17	12.4

[a]The model is fitted to the sticking model processed INMS E3, E5 data and the original UVIS E2 data.
[b]A plume sources rate is measured in s^{-1}.
[c]Bulk velocity of a gas in a plume in a vicinity of the surface is measured in ms^{-1}.
[d]Opening angle is defined by equation (1) and is measured in degrees.
[e]Zenith angle is measured in degrees between the vertical direction and the direction of the plume.
[f]Azimuth angle is measured in degrees clockwise from local north (that is, eastward to an observer standing on the surface facing north).

[29] Comparing parameters of individual sources, we have concluded that it is plumes I, II, III and VII that have the most contribution to the model results. Parameters only of those four plumes are presented in Tables 3 and 4. Although the other plumes do not contribute significantly to the present results, their input to the entire atmosphere is not necessarily negligible. It is possible that the influence of other plumes will dominate measurable data in other regions of the atmosphere and will be found during future flybys. But currently, there is no information that would allow determination of their parameters. For this reason, an estimate of the density distribution based on the upper limits for production rates of those plumes (Table 5) could be important for planning future flybys.

[30] Even though the description of the semi-analytical multi-plume model is given in terms of the first moments of a Maxwell-Boltzmann distribution function, instead of gas temperature it is an opening angle, α, that is used to characterize the plume in Tables 3 and 4. The reason for this is that the fitted temperature might be determined by local features of a vent that are not known. As a result, it is more illustrative to describe a plume in terms of an opening angle

$$\alpha = \tan^{-1} v_t / v_p, \tag{1}$$

which defines a cone that contains most of gas molecules injected by a plume. Here, v_p is a bulk speed of a gas flow injected by a plume, which is a parameter of the fitting procedure and $v_t = \sqrt{3kT_p/m_{H_2O}}$ is the mean thermal speed.

[31] The values of the opening angle obtained with the model are in a good agreement with those obtained from UVIS observations. Based on those observations, [*Hansen et al.*, 2008] determine a value of $v_p/v_t = 1.5$. This gives the opening angle, α, being about 34 degrees, which is consistent with the results of the model.

3.2. Test Particle Model

[32] Since gravity was excluded from consideration in the semi-analytical multi-plume model, it is necessary to check whether this assumption is valid. To do this, a test particle model was developed. Using parameters obtained with the semi-analytical multi-plume model, the density was recalculated. An example of such calculations is presented in Figure 1. Figure 1 shows a water density distribution in a plane that contains both, a trajectory of the spacecraft and the origin of a coordinate system related to the center of Enceladus. It can be seen that in the southern hemisphere, the density profile is dominated by the plumes. An enhancement of water density in the north pole region of Enceladus was an unexpected result of the simulation. As assumed before, the effect of gravity on high-speed particles can be neglected within the region of interest. But for those particles that compose the low energy part of the velocity distribution spectra, gravity is the force that determines its trajectory. The density enhancement that is seen in Figure 1 is due to particles with speed about or less than ~100 m s^{-1}.

[33] A comparison of results obtained with both models is presented in Figure 2. The agreement of density profiles obtained with two different methods shows that calculation of the density distribution in the southern hemisphere at typical flyby distance does not require accounting for the gravity force. On the contrary, a numerical simulation of a density distribution in the northern hemisphere requires accounting for the gravity force and has to be performed on a basis of kinetic theory in fully 3D geometry.

4. Conclusion

[34] The parameters of our semi-analytical model have been constrained by consistency with the original set of input Cassini data. Comparisons with the number and column densities for both cases are presented in Figures 3, 4 and 5. It can be seen that in the southern hemisphere outside of the area of the closest approach, the model results are within factor of ~2 from the input data. The fitted profile gets closer to the reference data with an increase of a distance between the spacecraft and Enceladus. Assuming that gas production does not change significantly over time, this implies that additional localized sources with smaller production rates than those of the considered plumes or some other atmospheric processes are important in the vicinity of Enceladus.

[35] The parameters used in the fitting procedure of the semi-analytical model are the first three moments of a Maxwell-Boltzmann distribution function. More physically correct and, possibly, realistic in terms of predicted density distribution, would be simulation of a gas in the vicinity of the vent instead of assuming a Maxwell-Boltzmann velocity

Table 5. Upper Limits of Source Rates of Plumes for Cases 1 and 2[a]

Plume	Case 1[b]	Case 2[c]
IV	3.0×10^{27}	2.1×10^{27}
V	6.4×10^{27}	3.5×10^{27}
VI	1.5×10^{27}	1.2×10^{27}
VIII	6.7×10^{27}	2.6×10^{27}

[a]Plume sources rate are measured in s^{-1}.
[b]The model is fitted to the original INMS E3, E5 and UVIS E2 data.
[c]The model is fitted to the sticking model processed INMS E3, E5 data and the original UVIS E2 data.

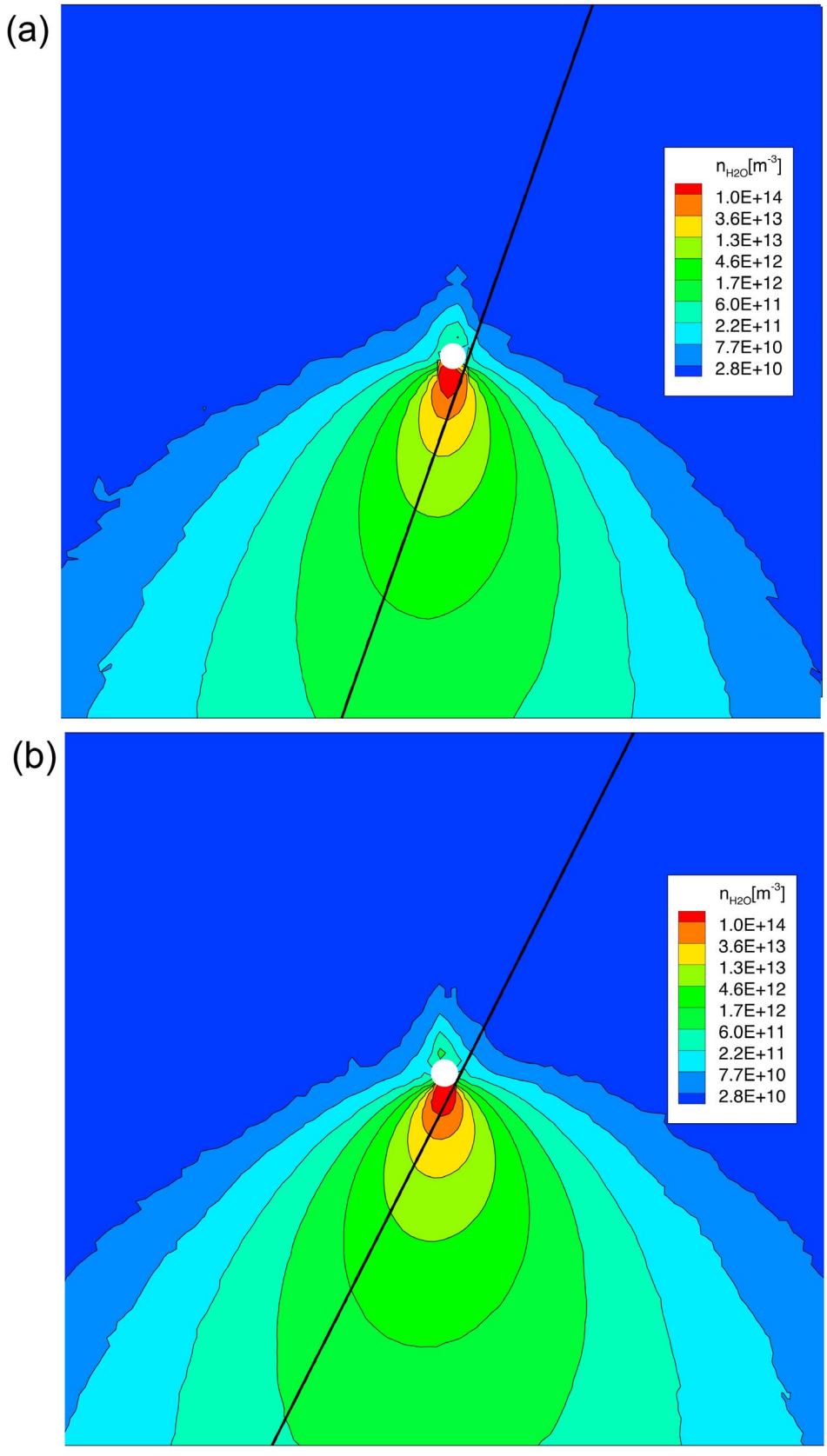

Figure 1. Distribution of water number density in a plane that contains trajectory of the spacecraft (the vertical black line) and an origin of a coordinate system related to the center of Enceladus. Presented distribution is obtained with the test particle Monte Carlo model for conditions corresponding to (a) E3 and (b) E5 flybys.

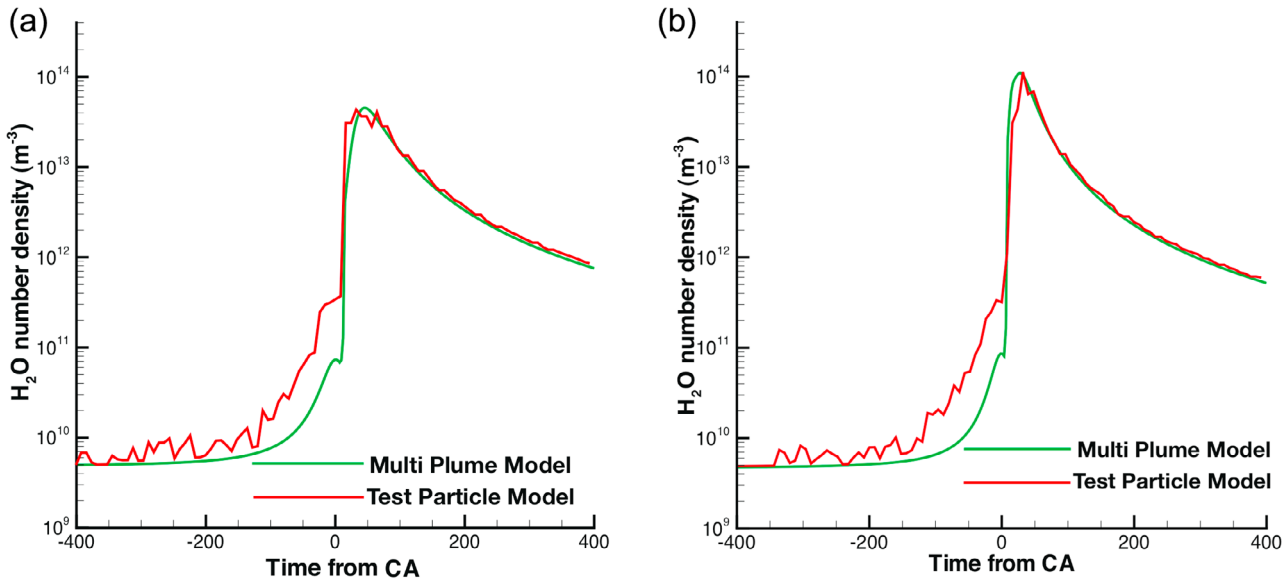

Figure 2. Comparison of model density profiles along (a) E3 and (b) E5 trajectories obtained with the test particle model and the multi-plume model fitted to the sticking model processed INMS E3, E5 and UVIS E2 data.

distribution. That could be done [*Combi*, 1996; *Crifo et al.*, 2005; *Tenishev et al.*, 2008] by solving the Boltzmann equation. The drawback of such an approach is a dramatic increase in computational cost in comparison with models presented here, together with the need for additional development of a model that would describe the interaction of gas flow with walls in a vent. At this point of our knowledge of Enceladus, such models can be only empirical. In other words, introduction of additional model parameters that are not determined from measurements will be required. That would not only complicate the global model, but also would raise a question of physical relevance of chosen values of the parameters.

[36] As noted above, the semi-analytical model allows us to calculate density within the atmosphere based on a set of model parameters obtained by a fitting procedure. It was found that only four sources contribute the majority of the gas measured by INMS E3 & E5, and the UVIS occultation. This doesn't mean that others sources are negligible in the global picture but rather that there is not enough information as yet to determine their parameters. But in the region nearby the considered trajectories and in the lines of sight of the UVIS column density measurements, other sources probably are not important. Given the consistency with the measurements, it is reasonable to conclude that the model produces a reasonably close general picture of the density distribution within the atmosphere of Enceladus and places reasonable estimates onto the source rates and opening angles of some of the major vents.

[37] The three flybys necessarily sample the plumes at both different times and different locations. Therefore the model, which is applied to all the data, is limited in providing a time-averaged picture of the global distribution. Examination of the individual model/data comparisons from flyby to flyby does show that some general conclusions of about the long term variability can be drawn. The model best fits the E3 INMS data, but is generally higher than the E2 UVIS data and lower than the E5 INMS data. This would indicate a possible long-term variability of the individual plumes caused by a change of their production rates or orientations.

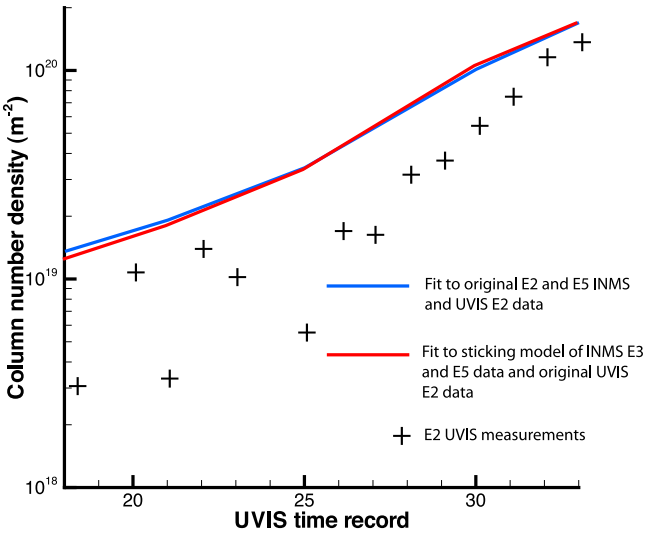

Figure 3. Water column density along the E2 trajectory. Comparison of the model result with the UVIS measurements.

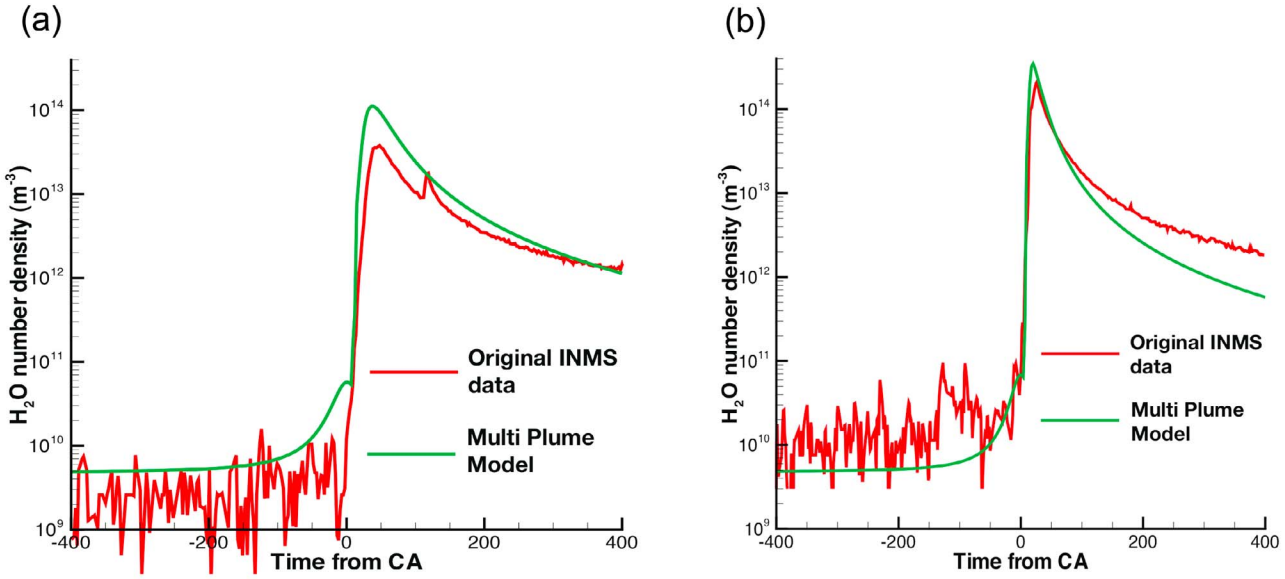

Figure 4. Water number density profiles along (a) E3 and (b) E5 trajectories. The model profile is obtained by fitting the original INMS E3, E5 and UVIS E2 data.

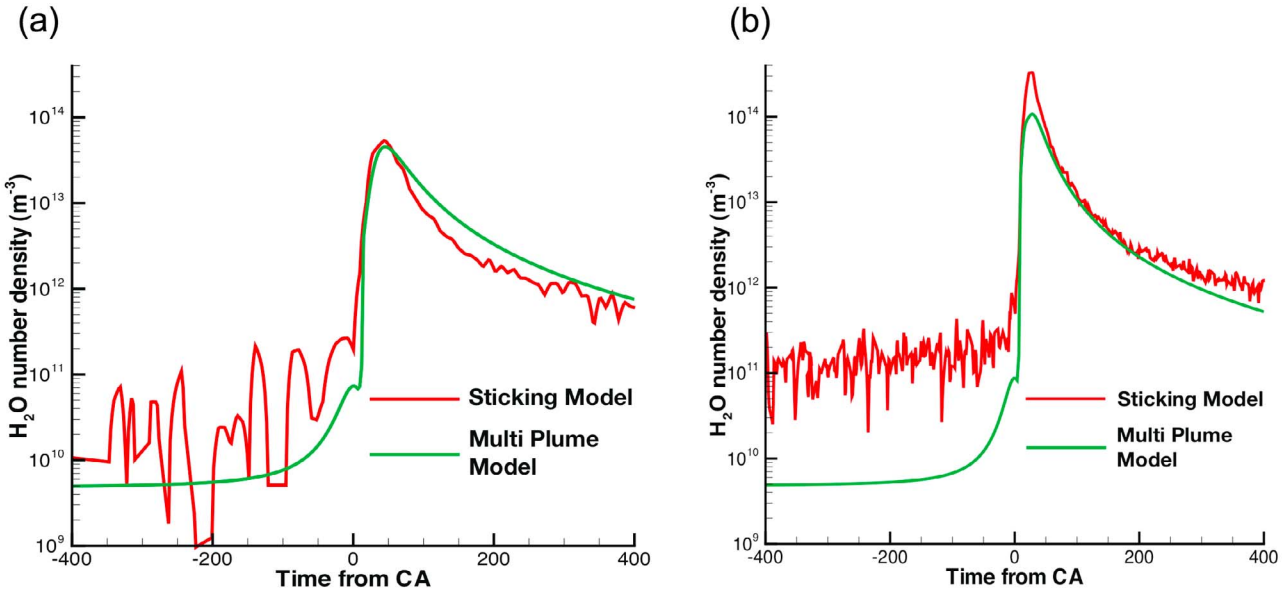

Figure 5. Water number density profiles along (a) E3 and (b) E5 trajectories. The model profile is obtained by fitting the sticking model processed INMS E3, E5 and the original UVIS E2 data.

[38] **Acknowledgments.** Support for this work was provided by grant NNX08AP94G from the NASA Cassini Data Analysis Program.

[39] Philippa Browning thanks Andrew Coates and another reviewer for their assistance in evaluating this paper.

References

Aristov, V. (2001), *Direct Methods for Solving the Boltzmann Equation and Study of Nonequilibrium Flows*, Kluwer Acad. Publ., Dordrecht, Netherlands.

Baum, W. A., T. Kreidl, J. A. Westphal, G. E. Danielson, P. K. Seidelmann, D. Pascu, and D. G. Currie (1981), Saturn's e ring, *Icarus*, *47*, 84–96.

Brown, R. H., et al. (2006), Composition and physical properties of Enceladus' surface, *Science*, *311*(5766), 1425–1428.

Buratti, B. J., J. A. Mosher, and T. V. Johnson (1990), Albedo and color maps of the Saturnian satellites, *Icarus*, *87*, 339–357.

Burger, M. H., E. C. Sittler, R. E. Johnson, H. T. Smith, O. J. Tucker, and V. I. Shematovich (2007), Understanding the escape of water from Enceladus, *J. Geophys. Res.*, *112*, A06219, doi:10.1029/2006JA012086.

Combi, M. (1996), Time-dependent gas kinetics in tenuous planetary atmospheres: The cometary coma, *Icarus*, *123*(1), 207–226.

Crifo, J., G. A. Loukianov, A. V. Rodionov, and V. V. Zakharov (2005), Direct Monte Carlo and multifluid modeling of the circumnuclear dust coma. Spherical grain dynamics revisited, *Icarus*, *176*(1), 192–219.

Dermott, S. F., and P. C. Thomas (1994), The determination of the mass and mean density of Enceladus from its observed shape, *Icarus*, *109*(2), 241–257.

Dougherty, M. K., K. K. Khurana, F. M. Neubauer, C. T. Russell, J. Saur, J. S. Leisner, and M. E. Burton (2006), Identification of a dynamic atmosphere at Enceladus with the Cassini Magnetometer, *Science*, *311*(5766), 1406–1409.

Hall, D. T., P. D. Feldman, J. B. Holberg, and M. A. McGrath (1996), Fluorescent hydroxyl emissions from Saturn's ring atmosphere, *Science*, *272*(5261), 516–518.

Hansen, C. J., L. Esposito, A. I. F. Stewart, J. Colwell, A. Hendrix, W. Pryor, D. Shemansky, and R. West (2006), Enceladus' water vapor plume, *Science*, *311*(5766), 1422–1425.

Hansen, C. J., et al. (2008), Water vapour jets inside the plume of gas leaving enceladus, *Nature*, *456*(7221), 477–479.

Harper, D., and D. Taylor (1993), The orbits of the major satellites of Saturn, *Astron. Astrophys.*, *268*, 326–349.

Hillier, J. K., et al. (2007), The composition of Saturn's e ring, *Mon. Not. R. Astron. Soc.*, *377*, 1588–1596.

Johnson, R. E., H. T. Smith, O. J. Tucker, M. Liu, M. H. Burger, E. C. Sittler, and R. L. Tokar (2006), The Enceladus and OH tori at Saturn, *Astrophys. J.*, *644*(2), L137–L139.

Jones, G. H., E. Roussos, N. Krupp, C. Paranicas, J. Woch, A. Lagg, D. G. Mitchell, S. M. Krimigis, and M. K. Dougherty (2006), Enceladus' varying imprint on the magnetosphere of Saturn, *Science*, *311*(5766), 1412–1415.

Jurac, S., M. A. McGrath, R. E. Johnson, J. D. Richardson, V. M. Vasyliunas, and A. Eviatar (2002), Saturn: Search for a missing water source, *Geophys. Res. Lett.*, *29*(24), 2172, doi:10.1029/2002GL015855.

Matson, D. L., J. C. Castillo, J. Lunine, and T. V. Johnson (2007), Enceladus' plume: Compositional evidence for a hot interior, *Icarus*, *187*(2), 569–573.

Meyer, J., and J. Wisdom (2007), Tidal heating in Enceladus, *Icarus*, *188*(2), 535–539.

Owen, T., D. Morrison, and L. Soderblom (1986), The satellites of Saturn, in *Satellites*, edited by J. Burns and M. Matthews, pp. 764–801, Univ. of Ariz. Press, Tucson, Ariz.

Porco, C. C., et al. (2006), Cassini observes the active south pole of Enceladus, *Science*, *311*(5766), 1393–1401.

Richardson, J. D., and S. Jurac (2004), A self-consistent model of plasma and neutrals at Saturn: The ion tori, *Geophys. Res. Lett.*, *31*, L24803, doi:10.1029/2004GL020959.

Shemansky, D. E., P. Matheson, D. T. Hall, H.-Y. Hu, and T. M. Tripp (1993), Detection of the hydroxyl radical in the Saturn magnetosphere, *Nature*, *363*(6427), 329–331.

Showalter, M. R., J. N. Cuzzi, and S. M. Larson (1991), Structure and particle properties of Saturn's E-Ring, *Icarus*, *94*, 451–473.

Smith, B. A., et al. (1981), Encounter with Saturn: Voyager 1 imaging science results, *Science*, *212*(4491), 163–191.

Spahn, F., et al. (2006), Cassini dust measurements at Enceladus and implications for the origin of the E-Ring, *Science*, *311*(5766), 1416–1418.

Spencer, J. R., et al. (2006), Cassini encounters Enceladus: Background and the discovery of a south polar hot spot, *Science*, *311*(5766), 1401–1405.

Spitale, J. N., and C. C. Porco (2007), Association of the jets of Enceladus with the warmest regions on its south-polar fractures, *Nature*, *449*, 695–697.

Squyres, S. W., R. T. Reynolds, and P. M. Cassen (1983), The evolution of Enceladus, *Icarus*, *53*, 319–331.

Tenishev, V., M. Combi, and B. Davidsson (2008), A global kinetic model for cometary comae. The evolution of the coma of the Rosetta target comet Churyumov-Gerasimenko throughout the mission, *Astrophys. J.*, *685*, 659–677.

Teolis, B., M. E. Perry, B. Magee, J. Westlake, and J. H. Waite Jr. (2010), Detection and measurement of ice grains and gas distribution in the Enceladus plume by Cassini's Ion Neutral Mass Spectrometer, *J. Geophys. Res.*, doi:10.1029/2009JA015192, in press.

Terrile, R. J., and A. F. Cook (1981), Enceladus: Evolution and possible relationship to Saturn's E-Ring, in *Lunar and Planetary Science XII, Supplement A. Satellites of Saturn*, Lunar and Planet. Inst., Houston, Tex.

Tian, F., A. I. F. Stewart, O. B. Toon, K. W. Larsen, and L. W. Esposito (2007), Monte Carlo simulations of the water vapor plumes on Enceladus, *Icarus*, *188*(1), 154–161.

Tokar, R. L., et al. (2006), The interaction of the atmosphere of Enceladus with Saturn's plasma, *Science*, *311*(5766), 1409–1412.

Waite, J. H., et al. (2006), Cassini ion and neutral mass spectrometer: Enceladus plume composition and structure, *Science*, *311*(5766), 1419–1422.

M. R. Combi and V. Tenishev, Department of Atmospheric, Oceanic and Space Sciences, University of Michigan, Ann Arbor, MI 48109, USA. (vtenishe@umich.edu)

B. D. Teolis and J. H. Waite, South-West Research Institute, San Antonio, TX 78228-0510, USA.